Size Scaling Relationships in the Active Fault Networks of Japan and Their Correlation With Gutenberg-Richter b-Values

Ali Osman Öncel[1,3], Thomas H. Wilson[2,] and Osamu Nishizawal[1]

[1]Geological Survey of Japan, Tsukuba 305-Japan

[2]West Virginia University, Dept. of Geology and Geography-USA

[3]Istanbul University, Dept. of Geophysical Engineering-Turkey

Abstract

Fractal properties of active fault systems in Japan are evaluated and compared to Gutenberg-Richter b-values. Properties of the active fault network and seismicity were evaluated at 20 km intervals along three lines oriented along the length of Honshu, the main island of Japan. Fractal dimensions for the active fault network are calculated using the box-counting method. The box curves often reveal the presence of an abrupt transition in slope at approximately 8 km scales. This transition separates linear regions in the box curves that span box sizes of 17.5-to-8.5 km and 7.75-to-2 km. Fractal dimensions were computed for the 17.5-to-8.5 km (D_L) and 7.75-to-2 km (D_S) range of box sizes from overlapping 70 x 70 km regions of the active fault complex. The maximum likelihood method is used to estimate b-value from earthquakes occurring in the seismogenic zone (upper 20 km).

The correlation between *D* and b-value varies considerably throughout Japan and can be either positive of negative. In general *D* and *b* are negatively correlated suggesting that increased complexity in the active fault network accommodates rupture along fault planes of relatively larger surface area. Significant positive correlations between *b* and *D* are also observed in Japan. Positive correlations occur in complex areas of the active fault network where the fractal dimension is highest. Here, the probability of large magnitude earthquakes decreases in response to increased fragmentation of the active fault network and increased possibility that stress release will take place along faults of smaller surface area. A negative correlation between *b* and *D* is also observed in the high *D* area of central Japan. The correlation suggests that higher magnitude intraplate seismicity should be expected, and indeed, higher magnitude seismicity is observed in this area. In another negative correlation area in southwest Japan, larger than average earthquake magnitude were not observed. The absence of larger than average magnitude earthquakes suggests that historical seismicity may, in itself, not provide an accurate estimate of the long-term probabilities of large intraplate earthquakes. The analysis may provide important insights into earthquake hazard assessment.

Introduction

In the following paper, we examine possible relationships between the distribution of active faults and recent seismicity along the Japan Island Arc. The majority of seismicity and faulting in the Japanese Islands appears to be related to the continuing movement of two arc systems (the Northeast and Southwest Japan systems) towards Eurasia (Figure 1). The Japanese Islands are divided geologically into two different tectonic regimes at about 138°E roughly separating SW and NE Japan. This line roughly falls along the Itoigawa-Shizuoka Tectonic Line, which serves as the western boundary of the Fossa-Magna region and eastern boundary of the Japan Alps. Seismicity in Japan is also categorized as intra-plate and interplate depending upon their tectonic origins. Intra-plate events are shallow events

that occur on land while the inter-plate events occur along major subduction zones such as those between the Philippine Pacific Sea plates along the Izu-Ogasawara Arc or along the Pacific and North American plates in northeast Japan. Earthquake recurrence for intra-plate events are much longer than inter-plate events (Shimazaki, 1978).

Seismotectonics of Japan are controlled in general by horizontal shortening. Compressional stress is oriented roughly E-W but can be quite variable. For example, in the Izu Peninsula area tectonic stress has a more northerly orientation in response to the collision of the Izu-Ogasawara Arc with central Japan in that area. The characteristics of faulting along the Japan Arc are very complex and have been divided geographically into several sub-fault systems. These include the main part of Hokkaido, the Inner and Outer belts of Japan, continental slopes of the Pacific coast of NE Japan, Northern tip of Izu-Ogasawara Arc, Western Fossa Magna belt, eastern and western parts of Inner belt of SW Japan, Median Tectonic Line belt, outer belt of SW Japan, continental slopes of the Pacific coast of SW Japan, the Ryuku Arc and Okinawa Trough (Research Group for Active Faults of Japan, 1995).

Analysis of active fault and seismicity data was conducted along lines that are oriented along the length of Honshu, the main island of Japan. Active fault patterns were analyzed using the box-counting method to compute size-scaling properties of the active fault network. Computations of fractal dimensions were made of 70 x 70 km regions spaced at 20 km intervals along each line. Seismicity along these lines was characterized using the Gutenberg-Richter b-value. This is one of the most widely used statistical descriptions of seismicity and is obtained from the frequency-magnitude relationship for earthquakes:

$$LogN = a - bm \tag{1}$$

where N is the number of events with magnitude greater than m, and a and b are constants. The Gutenberg-Richter relationship was shown by Aki (1981) to be the equivalent of a fractal distribution (Turcotte, 1997). Specifically it can be shown that the b-value is proportional to the fractal dimension in a power law relationship between the frequency of earthquake occurrence $\left(\dot{N}\right)$ and the area of fault rupture (A) such that

$$\dot{N} = \dot{b}\, A^{-b} \tag{2}$$

where $\dot{b}$ is a constant of proportionality (see Turcotte 1997). Since $A \propto r^2$, where r is a characteristic linear dimension of the fault surface, Equation 2 implies that $D = -2b$. This relationship has provided the basis for several studies including the present one. As Turcotte (1997) notes, the relationship implies one of two end member relationships: either there is a fractal distribution of faults, each having its own characteristic earthquake or that there is a fractal distribution of earthquakes along any given fault. We test the idea on a regional scale that the fractal distribution of earthquake frequency implied by the Gutenberg-Richter relationship is associated with a fractal distribution of faults.

In summary, seismicity can be related to the characteristic linear dimension of the active fault networks through a fractal relationship (Aki 1981). The main purpose of this paper is to evaluate whether such a relationship between seismicity and active faulting exists for the Japan Island Arc. Further, if a

relationship exists between these variables, how might such a relationship be pertinent to seismic hazard assessment?

Previous Works

Previous studies of the active faults in Japan by Hirata (1989a) and Matsumoto et al. (1992) suggest the active fault networks are fractal. Hirata's analysis covered most of Japan, and was conducted on 1 degree longitude by 40 minute latitude areas, roughly 90 by 74 km in size, using active-fault sheet maps of Japan published by the Research Group for Active Faults of Japan (1980). Matsumoto et al. (1992) analyzed narrow strip-like regions along the Median Tectonic line and the Izu Peninsula using data from the Research Group for Active Faults of Japan (1980) and also the Research Group for Active Tectonic Structures in Kyushu (1989). To estimate the fractal dimensions of active fault distributions, Matsumoto et al. (1992) employed a different method from the Hirata's method. Hirata used a box-counting method (e.g., Turcotte 1989, 1992), while Matsumoto et al. (1992) used the method of Okubo and Aki (1987) which is based on the relationship between the circle radius and the number of circles for covering the fault traces.

The results of Matsumoto et al. (1992) and Hirata (1989a) are not directly comparable, but, in general, both indicate similar fractal models of fault distribution, with a few exceptions. Matsumoto et al. (1992), for example, present the boxplot for an area along the Median Tectonic Line that is characterized by two linear regions in the log-log plots. Hirata (1989a) notes that a fractal relationship was not observed in several areas and excluded those regions from his analysis. Hirata's analysis of box-count data is restricted approximately to the 2-20 km range of scales, while the results of Matsumoto et al. (1992) appear to be restricted to the 1-10 km range of scales. Based on outcrop scale studies of fracture patterns in the North Izu Peninsula area, Hirata (1989a) suggested that the fractal characteristics of fractures on the 10-1 to 10-2 meter scale are similar to the larger scale active fault patterns. Hirata's results also indicate that the fractal dimensions of active fault systems are highest in central Japan and decrease toward southwest and northeast Japan.

The general form and physical significance of spatial and temporal fluctuations of the seismic b-value have been discussed by many authors (e.g., Gibovicz, 1973; Smith, 1986; Main et al. 1990; Main, 1992; Öncel et al. 1995, 1996a,b). Hirata (1989b) evaluated the relationship between Gutenberg-Richter b-value and the fractal dimension of focal point distribution. Hirata (1989b) found a negative correlation between the fractal dimension of focal point distributions and b-value for the temporal variation of seismicity in the Tohoku region of Japan. A similar relationship between seismic b-value and fractal dimension of the hypocenter distribution was obtained for the Parkfield area of California and northeastern Brazil (Henderson et al. 1992, 1994). Öncel et al. (1996a,b) observed a strong negative correlation between the seismic b-value and fractal dimensions of the temporal and spatial variations of seismicity in the North Anatolian Fault Zones (NAFZ). They pointed out that spatial variations of those parameters coincide with variation of geological structure or mechanical properties along the fault strike while their temporal variations are respectively consistent with stress intensity and greater clustering of seismicity (Main et al. 1990, Main et al. 1992). On the contrary, Öncel et al. (1995) concluded that systematic temporal changes of the latter parameters in the western part of NAFZ can be assigned to an artificial effect rather than to underlying tectonic mechanisms because upgrades in the seismic observation network led to temporal changes of the parameters. In the discussion about the relationship between seismic b-value and fractal dimension of focal point distributions, Xu and Xu and Burton (1999) pointed out the possibility that the result may depend on the earthquake magnitude range for which the analysis is undertaken. Their observations suggest that

seismic b-value varies from the macroscale (large m) and microscale (small m) regions. The macroscopic characteristics of seismicity observed in both Japan and along the NAFZ yield negative correlation between the fractal dimension of focal points and b-value, while the microscopic characteristics of seismicity for low magnitude events such as the cluster patterns of Brazil yield positive correlation. The observations of Xu and Burton (1999) suggest a scale-dependent relationship which is based on the occurrence of changes in "fractal" properties with scale range of seismicity, in contrast to the suggestions of Chen et al. (1998) and Kagan and Knopoff (1980) where the fractal characteristics of seismicity are magnitude independent.

Active Fault Analysis

Active Fault Data and Region of Analysis

Active faults analyzed in this study were digitized from revised editions of active fault maps (Research Group for Active Faults of Japan 1991) updated by the Geological Survey of Japan. Individual sheet maps cover 1° longitude by 40' latitude areas roughly 90 by 74 km at 1:200,000 scale. The active faults represented on these sheet maps portray all faults believed to have been active during the Quaternary (last 2 million years). Active faults are grouped into three categories depending on the certainty that movement actually occurred along any given fault during the Quaternary. In this study, we include all faults in our analysis so that our results can be compared directly to those of Hirata (1989a) who undertook the first comprehensive analysis of the fractal characteristics of faulting in Japan.

In order to portray variations in the fractal properties of the active fault network of Japan and relate them to seismicity via seismic b-value, the analysis was conducted along three lines (Figure 2) that extend along the length of Honshu. The analysis lines cross major tectonic subdivisions of Japan and the presentation of data along these lines yields continuous profiles of variation in fractal dimension and seismicity that cross major tectonic boundaries. The western end of each line is shared by lines 1 through 3 and extends about 440 km from the westernmost end of Honshu east to Kyoto and then continues along three separate branches. Line 1 continues eastward to Lake Kasumi (Kasumigaura), passing through the southern part of central Honshu. Lines 2 and 3 are almost parallel, cutting through central Japan and then continuing through northeast Honshu (Tohoku region). Line 2 covers the middle part of central Honshu and the eastern part of Tohoku (Outer side of Japan), whereas Line 3 covers the northern part of central Honshu and the western part of Tohoku (Inner side of Japan). In northeast Honshu (Figure 2), Line 2 lies to the east and Line 3 to the west.

Active fault analysis was conducted every 20 km along each line of 70 km x 70 km square regions centered at each analysis point. The sides of these square regions are oriented east-west and north-south. The lines were located so that the 70 x 70 km analysis regions in general did not extend beyond the coastline. Thus the effects of missing data and irregular geometry are minimized. With the exception of the first 70 km of each line, the covering boxes rarely extend beyond the coastline, and in those few exceptions, the initial covering box extends only a few kilometers beyond the coastline. Overlap in the area of analysis between successive analysis points also yields relatively smooth variation in calculated fractal dimension along each line.

Computation of Fractal Dimension for the Active Fault Pattern

In this study the box-counting method (e.g., Hirata 1989a; Turcotte 1989) is used to evaluate the detailed size-scaling characteristics of active fault networks in Japan. The fault pattern is covered by

square boxes with sides of length r and the number of boxes (N) containing part of the fault pattern are counted. If the pattern is fractal, then the number of occupied boxes (N) varies as the length of the box side (r) raised to some power ($-D$) as shown in Equation (2).

$$N = Cr^{b} \tag{3}$$

D is referred to as the fractal dimension, and C is a constant. As defined by Equation 3, D is a scale invariant parameter.

Box-counting analysis is illustrated using the active fault data of Iida (location shown in Figure 2). A close-up view of the fault pattern in the Iida area is shown in Figure 3A. Log transformation of Equation 2 yields a linear relationship between log$N$ and log$r$ with slope of $-D$. Number of occupied boxes (N) versus the box size (r) is plotted in a log-log scale (Figure 3B). Box counting of the Iida area was discussed and illustrated by Hirata (1989a) (see his Figure 2 for comparison). Hirata's estimate of D for the Iida area is 1.6, which was obtained from the 18.4-2.34 km range. Our estimate was made over a similar range, 17.5-2 km, and yielded D = 1.65. Hirata's analysis and that presented in Figure 3 are undertaken using a base 2 reduction in box size over the 18.4 to 2.34 km ranges. Thus the fractal dimension is computed from only 4 data points. In the current study we use a fractional box-counting algorithm (see Wilson 2000) that allows the size of the covering boxes to be adjusted using a noninteger base. Box size was decreased in equal logarithmic steps using a base approximately equal to 1.13. Base 1.13 decreases in box size yield 25 data points over the 17.5 to 2 km ranges. Recomputation of N and r from the Iida area using smaller logarithmic decreases in box size reveals significant nonlinearity in the log$N$/log$r$ plot of the Iida region (see Figure 4B). Two linear regions are observed (4B) with statistically different slopes of -1.88 " 0.036 and -1.45 " 0.023. Similar analysis is shown for the active faults mapped in the Hiroshima area (Figure 4C and D). Again, two nearly linear regions with statistically different slopes can be identified in the log$N$/log$r$ plots.

Sources of Error in Box-Counting Analysis

In our analysis, we have been careful to avoid features of the log$N$/log$r$ plots that are unrelated to the fundamental scaling properties of the pattern. For example, the initial (70 x 70 km) box will always be occupied since it covers the entire area. In the second covering, which consists in this example of four 35 x 35 km boxes, all boxes continue to be filled. When boxes at successively smaller scales are all occupied, the number of occupied boxes (N) increases as the square of the number of boxes along the map edge, and the number of boxes covering the map edge increases as $(l/r)^2$ yielding a log-log slope of -2 and fractal dimension of 2. The first 2 to 3 coverings of an area are commonly saturated with parts of the pattern. The steep slope (-2) observed (for example in Figure 3B) for the larger size boxes does not accurately characterize size-scaling attributes of the fault network at those scales. The first box covering counted in this analysis consists of boxes 17.5 km on a side and a total of 16 boxes. Some of the boxes usually become unoccupied at this scale.

Regions where D approaches 0 (e.g., Figure 3B) were also avoided in this analysis. The slope of the box curve decreases rapidly when the size of the box becomes less than the sampling interval used to digitize the fault traces. In this study, fault traces were digitized at approximately 200-m intervals. For box sizes less than the sampling interval, the number of occupied boxes will equal the total number of samples in the data set. Further decreases of box size yield no further increase in the number of occupied boxes and the slope of the curve in this region flattens out to 0 (Figure 3B).

If the data were comprised of continuous line segments, a reduction in box size by 1/2 would double the number of occupied boxes and we would eventually end up in a non-fractal region with D approaching 1 rather than 0. The scale at which this transition occurs may represent a resolution limit below which finer details are not represented, or are, in fact, not present. Fault patterns with $D \leq 1$ (e.g., Hirata 1989a) are also expected when the fault patterns appear as sets of disconnected segments which behave somewhat like the Cantor set.

Walsh and Watterson (1993) note these issues in their reevaluation of Pavement 1000 from Barton and Hseih (1989) in the Yucca Mountain area. Walsh and Watterson (1993) note that meaningful evaluations of a pattern's size-scaling attributes must be conducted in the zone between the transitional regions noted above to avoid sources of error associated with fracture trace digitization (or bitmap representations) and box saturation in the larger box coverings. Walsh and Watterson (1993) suggest that fractal analysis should be confined to the range of scales between the largest and smallest fracture spacing in the data set. A spacing of a kilometer or so represents an approximate minimum spacing for the active faults in the Iida area (Figures 3A and 4A). Maximum fault spacing reaches nearly 40 km or so between some of the smaller faults in the northwest quadrant of the area (Figures 3A and 4A). However, in this case, covering boxes greater in size than 17.5 km tend to be all occupied and thus yield a fractal dimension of 2 in the large r region of the log$N$/log$r$ plot. The range of box sizes (17.5 to 2 km) used in this study falls well within the range of scales accurately portrayed in the active fault maps.

Non-Fractal Behavior and Scale Transitions

Prior evaluation of non-linearity in the log$N$/log$r$ plots of the active faults in Japan (Wilson and Nishizawa 1998; Wilson 1999, 2000) generally found transitions between approximately linear regions at values of r between 6 and 9 km. These transitions are reminiscent of those found by Scholz (1995) using a power spectral analysis of surface roughness. Scholz noted the occurrence of both gradual and abrupt transitions in the fractal dimension with spectral wavelength. In his analysis of the surface rupture produced by the Dasht-e-Bayez earthquake of 1968 in Iran, Scholz (1995) found an abrupt transition in fractal dimension at 10 km scales. Scholz suggests that this transition is associated with the seismogenic thickness of the crust. Odling (1992) also notes the presence of slope breaks in his analysis of a single-fracture pattern. The break he observed is associated with the break from a slope of 2 observed with the larger box coverings. Odling (1992) notes that this break occurred approximately at the average spacing in the fracture pattern he analyzed. Recall from the discussion of error sources above, that the break from a slope of 2 occurs when box sizes become small enough that they fall into the spaces between fractures or clusters in the pattern and are unoccupied. Wilson (1999, 2000) evaluated the fractal characteristics of numerous fracture patterns in addition to the active fault patterns of Japan and found that slope transitions are a common attribute of log$N$/log$r$ plots. Model studies conducted by Wilson (1999, 2000) reveal that these transitions are associated with dominant or average spacing in the pattern of fractures at different scales and that more than one transition can occur. The slopes and thus the fractal dimensions are range-limited. Based on the analysis of log$N$/log$r$ plots from test areas, we estimate scaling parameters at two scales: one over the 17.5-to-8.5 km range and the second over the 7.75-to-2 km range. The range-limited fractal dimension over the 17.5-to-8.5 km range is referred to as D_L and that over the 7.75-to-2 km range, D_S. We follow the variations in D_L and D_S over these two scales and evaluate statistical relationships between the two along the entire length of Japan.

Analysis of the log$N$/log$r$ response over the 17.5-to-2 km region in several areas throughout Japan (for example, Figure 4) on average yielded slope transitions around 8 km. The 17.5-to-8.5 km and

7.75-to-2 km ranges provide a satisfactory representation of slope differences encountered in test areas. The correlation coefficients of regression lines fit to the data in these regions are all 0.99 or higher. Lei and Kusunose (1999) also identify two nearly linear regions in the log*N*/log*r* plots computed in their analysis of active fault networks of Japan. In their analysis they divided Japan into three areas. The analysis regions were approximately 550 km on a side and include extensive blank areas beyond the coastline and region of mapped faults. Transitions found in their analysis were located at approximately 13 km. However, it is difficult to compare their transition to that observed in the current analysis. The larger area of analysis and presence of extensive blank areas may account for the differences in the location of transitions observed in their log*N*/log*r* plots.

Regional Variations in Fractal Dimensions of the Active Fault Network

The general pattern of variation in D_L and D_S throughout Japan are illustrated for line 2 (Figure 5A). On all three lines taken together, D_L is on average 0.33 higher than D_S. Increases and decreases of the range-limited fractal dimensions along each line follow the increases and decreases in the intensity of faulting or total length of fault trace in any given analysis area. This is anticipated since the total line length (L) at a given scale (r) is just Nr. Substitution of N from Equation 3 yields $L = Cr^{1-D}$ From this relation, we find that the ratio of the length of fault traces (L_2) measured at scale r_2 to L_1 measured at scale r_1, grows as $(r_1/r_2)^{D-1}$. r_1 is the initial box size so that the ratio r_1/r_2 is always greater than 1.

Southwestern Honshu is relatively narrow and the analysis in this area was confined to one segment to prevent the 70 x 70 km analysis areas from extending beyond the coastline. In westernmost Honshu from 0 to 260 km (e.g., Figure 5), average D_L is 1.16. Average D_S in this same area is only 0.89. From 260 to 440 km < D_L increases to 1.71 and < D_S to 1.16. At both scales, the differences between D_L and D_S in these two areas of western Honshu are statistically significant at $\alpha = 0.01$ level based on the nonparametric Kolmogorov-Smirnov test. The range-limited fractal dimension of active fault patterns over the 17.5-to-8.5 km scale range (D_L) remain high with an average of 1.72 in central Japan west of ISTL, but drop to an average of 1.26 east of the ISTL. This difference is also significant at the $\alpha = 0.01$ level. Average D_L in northern Honshu drops further to 1.19. While < D_L in northern Honshu is less than that east of ISTL in central Japan, the difference is generally not statistically significant. The difference approaches significance ($\alpha = 0.1$) only when compared to D_L east of ISTL on Line 1. Here, D_L rises to 1.29.

Variations in D_S continue to follow D_L. Across the ISTL, D_S drops from an average of 1.34 to 1. The decrease continues into northeast Honshu where D_S drops to 0.88. Differences in D_S across the ISTL are significant at $\alpha = 0.01$. Differences in D_S between northeast Honshu and the region east of the ISTL in central Honshu are also significant at $\alpha = 0.01$ except for the region east of ISTL on Line 2. The region east of the ISTL (e.g., Figure 5) is a transitional region on all lines where D_L and D_S decrease in value. Along Line 2 the decrease is more abrupt so that D_L and D_S in this area differ little from those in northeast Honshu.

Error Analysis of D_L and D_S

Standard deviations in the estimates of D_L and D_S are compared for Line 2 (Figure 5B). On average, the standard deviations in the estimates of D are 0.03 for D_S and 0.09 for D_L. Standard deviations for D_S are fairly constant as shown for line 2 (Figure 5B), whereas those for D_L are quite variable. The standard deviations for estimates of D_L are much higher in the less intensely faulted areas of northeastern and southwestern Japan. Similar results are obtained along Lines 1 and 3. D_S is a more stable estimate

than D_L. The 95% confidence limits on the estimates of D_L and D_S are on average, 0.21 and 0.6, respectively. Given an average difference of 0.33 between D_L and D_S, the confidence limits on D_L and D_S make them on average statistically different at the 95% confidence level. In the remainder of this study we compare b-values only to D_S, since the precision of D_S, on average, is approximately three times that of D_L.

Earthquake Magnitude Analysis

Figure 6 shows the frequency-magnitude relation of events along Lines 1 through 3 for magnitudes greater than 2.5. In Figures 1 and 6, Lines 1 and 3 include a large number of great events with magnitudes 7 or greater. Along Line 2, which passes through central Japan and then goes out along the Outer (east) side of northern Japan, there are few events with the magnitude greater than 7. One possible interpretation of this difference is that the recurrence time of large earthquakes with magnitude greater than 7 may be longer than 400 years in the areas traversed by Line 2, since the time span of available data is only 400 years.

The analysis of earthquakes in this study was restricted to the zone of intraplate seismicity at depths $\leq$ 20 km. The thickness of the seismogenic zone in Japan is estimated to be approximately 15-20 km (Shimazaki, 1986; Zhao et al. 1992). Deep-seated earthquakes at depths greater than 20 km are most certainly linked to the interaction of the subducting plates of the Northeast and Southwest Japan rather than intraplate faulting. The data base used in this study was extracted from three earthquake data base including historical events: (1) Usami's (1996) historical catalogue from 1600 to 1884, (2) Utsds (1980) catalogue for the time period between 1885 and 1925, and (3) the instrumental catalogue compiled from the Japan Meteorological Agency (JMA) data file for the time period between 1926 and 1997. The compilation of the long-term seismic activity of Japan covering the past 400 years is considered to be complete. Figure 1 shows the hypocenter distribution.

The magnitude scale of historical data was taken from Utsu (1982) and Usami (1996) since they converted estimates of the magnitudes of historical events to the magnitude scale of JMA catalogue (Takashi Kumamoto, personal communication, 1999). We do not know the depths of these historical events but differentiate between intraplate and interplate events based on reports of damage associated with these events.

Only the main shocks, as selected by the Gardner's-Knopoff's (1974) procedure, were used in this analysis. The completeness for Usami's historical earthquake catalogue contains only the largest events (with M magnitudes equal to or exceeding 7.0) and provides information about long-term seismicity during the period from 1 January 1600 to 31 December 1884. The completeness for Utsu's catalogue includes all events of the magnitude equal to 5.7 or greater. More recent seismicity data is taken from the JMA database. The JMA database is divided into three subsets covering the period of time from 1 January 1926 to 31 December 1997. Data during the period extending from 1 January 1926 to 31 December 1977 includes complete coverage of earthquakes with magnitude equal to 4.1 and greater. The second part of the JMA catalogue (from 1 January 1978 to 31 December 1988) includes all earthquakes of magnitude equal to 2.8 or greater. The third part of the JMA catalogue (from 1 January 1988 to 31 December 1997) gives complete coverage of earthquakes with magnitude equal to 2.5 and greater.

Method of Analysis

Seismic b-Value

Seismic b-value is calculated using the maximum likelihood methodology by the use of unequal completeness periods for different magnitude thresholds (e.g., Kijko and Sellevoll, 1992; Öncel et al. 1996).

Seismic b-value may be estimated by the use of different methodologies such as maximum likelihood and least square. In this study, the Maximum Likelihood Methodology (MLM) is preferred to compute seismic b-value since it is reported to be a more appropriate way to compute a better estimation of b-value since it is inversely proportional to the mean magnitude (Utsu, 1965; Aki, 1965):

$$b = \frac{\log_{10} e}{\overline{m} - m_0} \tag{4}$$

where $\overline{m}$ is the average magnitude of events exceeding a threshold magnitude (m_0) for complete reporting of earthquake magnitudes and $log_{10}\, e = 0.4343$. A stable estimation of the b-value by the MLM requires at least 50 events (Utsu, 1965). The standard deviation (δb) of seismic b-value in 95 percent confidence limits may be determined using the equation suggested by Aki (1965):

$$\delta b = 1.96\, b / \sqrt{n} \tag{5}$$

Estimates of b-value were made in cylindrical volumes of radius r equal to 50 km and height h equal to 20 km. The centers of each cylindrical region were positioned at 20 km intervals along each of the three lines (Figures 1 and 2). Seismic b-value was calculated for each volume along the profile.

Variations of b-Value

The increase and decrease of b-values along each line in general follow the visual density of the seismicity pattern (Figure 1). In westernmost Honshu from 0 to 260 km along Line 1 (e.g., Figure 7A), the average b is 0.62 " 0.06. From 260 to 440 km < b decreases to 0.51 " 0.04. Average b in Line 2 from 500 to 900 km (Figure 7B) increases further to 0.64 " 0.06 while it drops further to 0.56 " 0.05 in Line 3 from 440 to 792 km and 0.49 " 0.05 in Line 1 from 500 to 800 km. The b-values in Line 1 from 820 to 840 have higher standard errors (approximately 0.4 and 0.5) since the number of events in this area is less than 10.

Seismic b-values computed in this study may have possible artifacts associated with systematic temporal variations in the pattern of earthquake location and station coverage that is difficult to assess. However, any such fluctuations are likely to have affected the results in a similar way for each profile, and we have attempted to minimize such artifacts by choosing largest events, which are more likely to be completely reported. In the present comparative study, the effect of any such artifacts is, therefore, more likely to affect the absolute values of the parameters rather than their relative values.

b-Value Error Analysis

Standard deviations in the estimates of b-value are compared for each line (Figure 7B). The standard deviations in the estimates of *b* are on average, 0.05 for Line 1, and 0.06 for Lines 2 and 3. Standard deviations for b-value are fairly constant along the length of Line 2. The standard deviations for estimates of b-value are much higher in the less seismically active areas of northeastern and southwestern Japan but the differences on average (0.01) are not so significant.

Correlation Analysis Between b-Value and Fractal Dimension

Gutenberg-Richter b-value is used to define changes of seismicity observed along each analysis line. In general, regions characterized by high b-value have a greater proportion of low-magnitude earthquakes while areas of low b-value represent areas where large magnitude earthquakes are more likely. Areas in the active fault network characterized by higher *D* are associated with greater complexity in the fault pattern and a persistence of this complexity at smaller scales. As noted earlier, increases in *D* are in general related to increases in the total length of faults over the 7.5 to 2 km scales.

Comparison of Gutenberg-Richter b-values and D_S along Lines 1 through 3 yields negative correlation. The correlation coefficient between *b* and D_S along Line l is -0.35. Along Lines 2 and 3, the correlations are -0.12 and -0.33, respectively. Examination of Figure 7 reveals that increases in D_S are often associated with decreases in b-value. We suggest that a negative correlation is, in general, to be expected for the following reasons. A decrease in *b* is associated with increased probability of larger magnitude earthquakes, while increases of *D* indicate increased fault length. The general tendency for *b* to decrease when D_S increases suggests that there is increased probability that stress release will occur with through rupture along faults of greater length and, therefore, greater surface area.

Figure 7 reveals that there is considerable spatial variability in the relative changes of *b* and D_S, We wished to evaluate this relationship at a more local level throughout Japan to determine if variations in the correlation might be related to the major tectonic subdivisions in Japan. To do this, we compared D_S and *b* along Lines 1 through 3. Correlation coefficients between D_S and *b* were computed at 20-km intervals along each line. As noted, *b* was computed from seismic events located in cylindrical regions with radius of 50 km and depth of 20 km. D_S was computed at the same points from active faults in 70 x 70 km size square regions. Although the analysis is presented along lines, the data are representative of large areas and volumes centered on each line.

A local measure of the correlation between *b* and D_S was computed using a 160-km long sliding window. The local correlation is plotted along each line in Figure 7 and is contoured in Figure 8. The local correlation (Figures 7 and 8) reveals large regions of negative and positive correlation throughout Japan (Figure 8). One zone of positive correlation (Area II) extends north-south through central Japan (Figure 8). Just to the east, across the ISTL, this zone of positive correlation changes abruptly to a zone of low correlation. The ISTL marks the location of an incipient subduction zone between the Eurasian plate (to the west) and the North American Plate (to the north). The area west of the ISTL in central Japan coincides with the most intense concentration of Quaternary faults (Wesnousky et al. 1984) (also see Figure 2). These 160-km windows of data included 9 data points. Examples of the relationship between D_S and *b* are illustrated in Figure 9. The examples are taken from positive correlation Areas I, II, and III. In the following discussion, we examine the different areas of positive and negative correlation and consider their statistical as well as seismotectonic significance.

Discussion

The comparison of b-value to D_S reveals regions of both positive and negative correlation (Figure 8). These regions are extensive and in central Japan reveal consistency from line to line. In the following discussion, we evaluate the possible significance of the correlations beginning first with southwestern Japan and proceeding through central Japan into northeastern Japan.

A small region of positive correlation appears on the southwestern end of Line 1. The correlation occurs in response to a parallel rise and fall in the value of D_S and b along the first 100 km of the line (Figure 7). D_S varies from approximately 0.8 to 1.2. Standard deviations on the estimates of D_S are approximately 0.03. The difference in D_S exceeds the standard deviation in the estimate over 13 times and is considered significantly different. The variation of b through this region is at most 0.2. Standard deviation in the estimate of b in this area is approximately 0.1. The 0.2 variation in b differs by at most two standard deviations. The fluctuations in b are, however, quite variable and the resulting correlation between D_S and b is not considered significant.

To the east at about 200 km along Line 1, the correlation coefficient drops approximately to -0.8. This zone of negative correlation develops in response to an increase in D_S and parallel decrease in b-value. In this case the drop in b is approximately 0.45. The standard deviations of the estimates of b in this area are only 0.05; hence, the drop in b-value is considered significant. The variations in D_S also form a statistically significant positive trend. Excluding the extremely low value of D_S (0.3) at approximately 160 km out along the line, D_S increases approximately from 0.7 to 1.1 (13 standard deviations). Since the rise and fall of D_S and b (respectively) are statistically significant, the negative correlation that arises around 200 km is also considered to be statistically significant.

The drop in b implies a relative increase in the probability of larger magnitude earthquakes. The decrease in b with increase in D_S suggests that in this increasingly deformed area fault planes may have greater surface area and give rise to earthquakes of greater magnitude. However, maximum earthquake magnitudes in this area (see Figure 10) tend to be on average about 6. The coincidence of increased fault complexity with lower b-value and relatively low historic earthquake magnitudes suggests that there is increased probability of larger magnitude earthquakes occurring in this area.

Continuing farther to the east, we examine the west-to-east rise in the local correlation observed through Area I (see individual line plots, Figure 7). On Line 2 for example, D_S increases approximately from 0.7 to 1.25 through the region of positive correlation. Given average standard deviations in the estimate of D_S, the 0.55 increase in D_S is considered statistically significant. Values of b increase from approximately 0.3 to 0.65. The standard deviations of b in this area are approximately 0.05 so that this positive trend in b is also considered significant. Since the west-to-east increases in b and D_S are both statistically significant, the positive correlation between b and D_S is also considered significant.

The rise in D_S indicates increased complexity in the active fault complex. The concomitant rise in b suggests decreased probability of higher magnitude earthquakes. Earthquake magnitudes in the area are again approximately 7 on average. In this case, the increasingly complex active fault network may accommodate stress release on faults of smaller surface area.

Positive correlation Area II develops from an east-to-west rise in both b and D_S. The east-to-west rise in D_S is significant on all three lines (see Figure 7). The significance of the rise in b is questionable on Lines 1 and 2, but the 0.4 to 0.7 rise in b-value along Line 3 from 650 to 500 km is significant. The

significance of the positive correlations in the southern part of Area II may be questionable, but that in the northern part of Area II is not. In general these positive correlations appear to be associated with transitions from sparse to dense areas in the active fault network accompanied by decreased probability of larger magnitude earthquakes. Area II coincides with areas where the maximum earthquake magnitude is generally lower than in surrounding areas (Figure 10) and provides support for the lowered probability of larger earthquakes. The coincidence between increased complexity in the active fault network and lowered probability of larger earthquakes suggests that, as in Area I, stress release is accommodated on faults of smaller surface area.

Between Areas I and II, we find an area of negative correlation extending from about 350 to 600 km on all three lines (Figures 7 and 8). The west-to-east decrease in b between 375 to 475 km on Line 3, for example, is from approximately 0.7 to 0.45. D_S increases from approximately 1.25 to 1.45. In both cases, the change is significant over this region of negative correlation. The differences in b observed to the south on Lines 1 and 2 are smaller and of questionable significance. We consider the northern extent of the negative correlation area along Line 3 to be significant. The decrease of b into the center of the area suggests an increased probability of higher magnitude earthquakes. Examination of the active fault complex in Figure 2 indicates that the region of negative correlation is associated with an intensely faulted area between the 400 and 500 km markers (Figures 2 and 7). Note that the areas west and east of this 400 and 500 km are less intensely faulted and associated with a reduction in D_S to either side of the point located at 450 km in Lines 1 through 3 (see individual line plots in Figure 7). Stresses building up in this region may be concentrated in this more intensely faulted area, giving rise on average to higher magnitude earthquake activity. An increased probability of large earthquakes in this area is confirmed in Figure 10 where larger magnitude earthquake activity forms a distinct trend that coincides with this area of negative correlation (Figure 8).

The area of negative correlation lying just east of the ISTL arises from significant differences in b and D_S along Lines 2 and 3. D_S drops to the east across the ISTL as b increases. In general we would expect this increase in b to indicate reduced probability of larger magnitude earthquakes; however, in the present case, the maximum magnitude of earthquakes in this region is slightly greater than in Area II just to the west (Figure 10).

A third zone of positive correlation (Area III) is observed along Line 2 in northeastern Japan. The positive correlation between 775 km and 975 km is loosely associated with a parallel rise and fall of D_S and b centered at about 800 km along the line (just west of 900-km mark on Figure 2). The rise and fall of b in this area (see Figure 7) is significant, but the variations of D_S (0.1 at most) are quite small and of questionable significance. In general, throughout this region of positive correlation, the variations of D_S are small and erratic and we do not consider it further. However, if we were to consider that Area III was indeed a significant area of positive correlation throughout, we might reason that the fault pattern in this area becomes less complex because the details of the pattern are obscured by recent sedimentation or other factors such as the presence of blind faults and unmapped faults in rugged terrain. An incomplete representation of the active fault network will yield a lower for D and could possibly give rise to correlations between b and D. Other regions of positive and negative correlation appearing farther to the north along Lines 2 and 3 (Figure 8) lack statistical significance and are not discussed.

Summary and Conclusion

We have analyzed seismicity data covering a period between 1600 and 1997 to examine the spatial variations of the Gutenberg-Richter b-value and the size-scaling attributes of the active fault networks

observed along three lines (Figure 2) that extend along the length of Honshu, Japan. We used the methods of box counting and maximum likelihood for analyzing the complexity of the fault network and the rate changes of seismicity, respectively.

Detailed box counting of the active fault patterns in Japan over the 17.5 km to 2 km range yields two linear regions in the log$N$ and log$r$ box curve. These linear regions are separated by an abrupt transition located at approximately 8-km scales. The non-linear behavior over the 17.5 to 2 km scale range indicates that the fault network is not truly fractal or possesses only range-limited fractal properties. We were careful to avoid possible sources of error associated with data sampling and box saturation in the larger box coverings. The range-limited fractal dimension over the 17.5-7.5 km (D_L) is almost always statistically greater than the range-limited fractal dimension computed over the 7.5-2 km scale (D_S). The standard deviations in the estimates of D_S (0.03) are considerably less than those for D_L (0.09) so that D_S was used to represent the variations in complexity of the active fault network.

Overall there is a negative correlation between the Gutenberg-Richter b-value and the active fault size scaling parameter (D_S) along each of the three profiles. The correlations between D_S and b on Lines 1 through 3 are -0.35, -0.12, and -0.33, respectively. Negative correlation between b and D_S suggests that increases in the complexity of the active fault network (higher D) are, on average, associated with increased probability of occurrence of larger magnitude earthquakes (lower b) and vice versa. This relationship suggests that increased fault complexity (increased D_S) increases the interconnections between faults and thus increases the total fault surface area along which fault rupture can occur. In general the larger the fault-rupture area, the larger the magnitude of the earthquake (e.g., Turcotte, 1997).

Computation of local correlation between b and D_S using a sliding 160-km long window reveals that negative correlation does not persist at more local scales (Figures 7 and 8). Regions of local positive and negative correlation are observed. We suggest that positive correlation Areas I and II (Figure 8) occur when fault complexity (larger D_S) becomes so great that it is possible to accommodate stress release on smaller faults. It becomes increasingly unlikely in these areas that fault rupture will occur along one, through-going fault surface. The fault network is too fragmented. The net result is that these areas, which are exceptions, are characterized by relatively lower magnitude seismicity. One additional area of positive correlation (Area III) was also observed in the data. Although significant variations of b occur through this area, in general, we discount the significance of this positive correlation area because the variations of D_S are relatively small and erratic.

The negative correlations occurring in southwest and across the ISTL in central Japan result where b decreases along with an increase in D_S. These relative changes would appear reasonable on a tectonic basis. It seems likely that as the fault system varies spatially from a relatively sparse and fragmented network (D_S less than 1) to one in which the faults become more continuous and numerous (D_S greater than 1), that the probability of larger earthquakes will increase (smaller b-value). The possibility of rupture occurring on fault planes of larger surface area will increase with D_S, but only to a certain point. Further increases in D_S, as occur in Areas I and II, are associated with increases in b. In these cases, the fault network may be so interconnected that the likelihood of failure along large surface area is diminished. More intensely deformed areas provide an abundance of smaller faults along which strain can be dissipated so that the probability of larger magnitude earthquakes decreases.

The foregoing comparisons yield a measure of the correlation of short-term seismicity, represented by b-value with long-term deformation, represented by D_S (the range-limited measure of the fractal

distribution of active faults in Japan). The possible tectonic meaning of these areas of positive and correlation is speculative. However, we have been able to show that present day seismicity as measured through b-value changes significantly over distances of 100-200 km and that these changes correlate negatively or positively with the changes in the distribution of active faults represented by their range-limited fractal properties. Our observations suggest that examination of detailed variations in the correlation between *b* and *D* may provide insights into the seismic hazard assessment of active tectonic areas. The negative correlation occurring just west of Area I is associated with relatively low maximum magnitude earthquake activity. Yet, this area has lower b-values than occur elsewhere in Japan and coincides with an area of increased active fault complexity. The lower maximum magnitudes of earthquakes in this area may represent anomalous conditions. The coincidence of low maximum magnitude and low b-value may in itself suggest that historical earthquake activity in this area may not be representative of the potential for greater earthquakes. However, an active fault network of increasing complexity is present through the area along which larger magnitude earthquakes could occur.

Acknowledgements

We are grateful to Dr. Kano, Dr. Tanaka, Dr. Kato, and Dr. Kijko for their review of the paper and constructive comments. We would also like to thank Dr. Wiemer for providing us the software of ZMAP that was effectively used for the computation of seismic b-value. This study was supported in part through an AIST (Öncel) and STA (Wilson) fellowships. The size-scaling analysis of active fault networks presented in this paper was supported in part through U.S. Department of Energy grants DE-FG21-95MC32158 and DE-FG26-98FT40385. Discussions with Tom Mroz, Royal Watts, and Bill Gwilliams of the Morgantown Federal Energy Technology Center were also much appreciated.

References Cited

Aki, K., Maximum likelihood estimate of b in the formula log N = a - b M and its confidence limits, *Bulletin of the Earthquake Research Institute, 43*, 237-239, 1965.

Aki, K., 1981, A probabilistic synthesis of precursory phenomena: in Earthquake *Prediction: An International Review*, *Maurice Ewing Ser*., Vol. 4, edited by D.W. Simpson and P.G. Richards, p. 566-574.

Barton, C.C., and Hseih, P.A., 1989, Physical and hydrologic- flow properties of fractures; 28th International Geological Congress Field Trip Guidebook T385, *American Geophysical Union*, Washington, D.C., p. 36.

Chen, Y., Chen, L., and Wu, R., 1998, A new fractal apporoach to the clustering of earthquakes: physical fractal, *Bulletin of Seismological Society of America*., vol. 88, p. 89-94.

Gardner, J.K., and Knopoff L., 1974, Is the sequence of earthquakes in southern California, with aftershocks removed, poissonian?, *Bulletin of Seismological Society of America*. 1974. Vol. 64, p. 1363-1367.

Gibovicz, S.J.,1973, Variation of the frequency-magnitude relation during earthquake sequences in New Zeland, *Bulletin of Seismological Society of America*. 63, 517-528.

Hirata, T., 1989a, Fractal dimension of fault systems in Japan: Fractal structure in rock fracture geometry at various scales: *Journal of Pure and Applied Geophysics*, Vol. 131, Nos. 1/2, p. 157-170.

Hirata, T., 1989b, Fractal dimension of fault systems in Japan: Fractal structure in rock fracture geometry at various scales: *Journal of Geophysical Research*, Vol. 94, p. 7507-7514.

Henderson, J.R., Main, I.G., Meredith, P.G., and Sammonds, P.R., 1992, The evolution of seismicity at Parkfield, California observation, experiment, and a fracture - mechanical interpretation. *Journal of Structural Geology*., Vol. 14, Nos. 8/9, p. 905- 914.

Henderson, J.R., Main, I.G., Takaya, M., and Pearce, P.R., 1994, Seismicity in northeastern Brazil - fractal clustering and the evolution of the b-value. *Journal of Geophysical International*, Vol. 116, p. 217-226.

Kagan, Y.Y., and Knopoff, L., 1980, Spatial distribution of earthquakes: the two point correlation function, *Journal of Geophysical Royal Astronomical Society*., Vol. 62, p. 303 -320.

Kijko, A., Sellevoll, M.A., 1992, Estimation of earthquake hazard parameters from incomplete data files, Part II, Incorporation of magnitude heterogeneity. *Bulletin. Seismological Society of America*., Vol. 82, p. 120-134.

Lei, X., and Kusunose, K., 1989, Fractal structure and characteristic scale in the distributions of earthquake epicenters, active faults, and rivers in Japan: Geophys. J. Int., 13 p plus 9 Figures, in press.

Main, I.G., Meredith., P.G., Sammonds, P.R., and Jones, C., 1990, Influence of fractal flaw distributions of rock deformation in the brittle field. In deformation Mechanisms, Rheology and Tectonics (eds. Knipe, R.J., and E.H. Rutter), *Geological Society of London*, Special Publication 54, p. 81-96.

Main, G., Meredith, P.G., and Sammonds, P.R., 1992, Temporal variations in seismic event rate and b-values from stress corrosion constitutive laws. *Tectonophysics*., Vol. 211, p. 233-246.

Main, I.G., 1992, Damage mechanics with long-range interactions: correlation between the seismic b-value and the two-point correlation dimension. *Journal of Geophysical International*, Vol. 111, p. 531-541.

Matsumoto, N., Yomogoda, K., and Honda, S., 1992, Fractal analysis of fault systems in Japan and the Philippines: *Geophysical Research Letters*, Vol. 19, No. 4, p. 357-360.

Odling, N.E. Network properties of a two-dimensional fracture pattern. Pageoph., Vol. 138, p. 95-114,1992.

Öncel, A.O., Alptekin, Ö., Koral, H., 1998. The Dinar earthquake of October 1, 1996 (M_w = 6.2) in southwestern Turkey and earthquake hazard of the Dinar-Civril fault, *Journal of Pure and Applied Geophysics*, Vol. 152, p. 91-105.

Öncel, A.O., Main, I., Alptekin, Ö., Cowie, P., 1996a, Spatial variations of the fractal properties of seismicity in the Anatolian Fault Zones, *Tectonophysics*, Vol. 257, p. 189-202.

Öncel, A.Ö., Main, I., Alptekin, Ö., Cowie, P., 1996b. Temporal variations of the fractal properties of seismicity in the north Anatolian fault zone between 31°E and 41°E, *Journal of Pure and Applied Geophysics*. Vol. 146, p. 147-159.

Öncel, A.O., Alptekin, O., Main, I., 1995. Temporal variations of the fractal properties of seismicity in the western part of the north Anatolian fault zone: possible artifacts due to improvements in station coverage, *Journal of Nonlinear Processes in Geophysics*, Vol. 2, p. 147-157.

Okubo, P., and Aki, K., 1987, Fractal geometry in the San Andreas Fault system; *Journal of Geophysical Research*, Vol. 92, No. B1, p. 345-355.

Research Group for Active Faults of Japan, 1995, Maps of active faults in Japan with an explanatory text, *University of Tokyo Press*.

Research Group for Active Faults of Japan, 1980, Active faults in Japan: Sheet maps and inventories: (in Japanese) revised edition, *University of Tokyo Press*, 363 p.

Research Group for Active Faults of Japan, 1991, Active faults in Japan: Sheet maps and inventories: (in Japanese), revised edition, *University of Tokyo Press*, 437 p.

Research Group for Active Tectonic Structures in Kyushu, 1989, Active tectonic structures in Kyushu, Japan: (in Japanese), *University of Tokyo Press*, 553 p.

Research Group for Quaternary Tectonic Map, 1973, Quaternary tectonic map of Japan, map and explanatory text of the National Research Center, Disaster Prevention, 167 p.

Scholz, C.H., 1995, Fractal transitions on geological surfaces: in Fractals in the Earth Sciences, C.C. Barton and P. LaPointe, Editors, Plenum Press, New York, pp. 131-140.

Shimazaki, K., 1978, Correlation between intraplate seismicity and interplate earthquakes in Tohoku, Northeast Japan, *Bulletin of Seismological Society of America*. 68, 181-192.

Shimazaki, K., 1986, Small and large earthquakes: The effects of thickness of the seismogenic layer and the free surface, in Earthquake Source Mechanics. AGU Geophys. Mono. 37, edited by J.B.S. Das and C. Scholz, p. 209-216, American Geophysical Union, Washington, D.C.

Smith, W.D., 1986, Evidence for precursory changes in the frequency-magnitude b-value, *Journal of Geophysical Royal, Astronomical Society*, Vol. 86, p. 815-838.

Turcotte, D.L., 1989, Fractals in geology and geophysics; Pure and Applied Geophysics, p. 171-196.

Turcotte, D.L, 1992, Fractals and chaos in geology and geophysics: *Cambridge University Press*, 221 p.

Turcotte, D.L, 1997, Fractals and chaos in geology and geophysics: Cambridge University Press, Cambridge, 2nd edition, 398 p.

Usami, T. Materials for Comprehensive List of Destructive Earthquakes in Japan. Tokyo: Tokyo Press, 1996.

Utsu, Catalog of large earthquakes in the region of Japan from 1885 through 1980, *Bull. Earthq. Res. Inst., Univ. Tokyo*, 1982 (**57**):401-463.

Utsu, T., 1965, A method for determining the value of b in a formula log n = a - bM showing the magnitude frequency for earthquakes, *Geophys. Bull. Hokkaido Univ*., Vol. 13, p. 99-103.

Xu, Y., and Burton, P.W., 1999, Spatial fractal evolutions and hierarchies for microearthquakes in central Greece, *Journal of Pure and Applied Geophysics*. Vol. 154, p. 73-99.

Walsh, J.J., and Watterson, J., 1993, Fractal analysis of fracture patterns using the standard box-counting technique: valid and invalid methodologies, *Journal of Structural Geology*, Vol. 15, No. 12, p. 1509-1512.

Wesnousky, S.G., Scholz., C.H., Shimazaki, K., and Matsuda, T., 1984, Integration of geological and seismological data for the analysis of seismic hazard: A case study of Japan, *Bulletin of Seismological Society of America*., Vol. 74, p. 687-708.

Wilson, T.H., Dominic, J., and Halverson, J., 1997, Fractal interrelationships in field and seismic data: Final Research Report of Work Conducted on DOE Contract DE-FG21-95MC32158, 162 p.

Wilson, T.H., and Nishizawa, O., 1998, Fractal interrelationships between active fault patterns and topography in Japan: Interim report on NSF/STA Short Term Fellowship - Fractal interrelationships between surface topography, active fault patterns and seismicity in Japan, 20 p. plus 13 figures.

Wilson, T.H. 1999, Non-fractal size-scaling attributes of fracture trace and active fault networks with examples from the central Appalachians and Japan: in GSA Abstracts with Programs, Vol. 31, No. 7, p. Al12.

Wilson, T.H., 2000, Size scaling relationships in fracture networks: Final Research Report of Work Conducted on DOE Contract DE-FG26-98FT40385, 89 p.

Wilson, T.H., in review, Scale transitions in fracture and active fault networks: Mathematical Geology, 40 p.

Zhao et al. 1992, Seismic velocity structure of the crust beneath the Japan Islands, *Tectonophysics*, Vol. 212, p. 289-299.

Figure Captions

Figure 1: Shallow seismicity data (h < 40 km) on land covering the period of time from 1600 to 1997.

Figure 2: Active fault map of Honshu and Shikoku. Locations of analysis Lines 1 through 3 are shown.

Figure 3. Frequency-magnitude distributions for 100 km wide bands of seismicity centered on each of lines through 1 to 3.

Figure 4: (A) Active faults of the Iida area located in central Japan (Figure 1). (B) log$N$/log$r$ plot of the active fault network in Iida. (C) Local slope variations between adjacent points of the log$N$/log$r$ plot. (Taken from Wilson et al. [1996]).

Figure 5: Log$N$/log$r$ plots computed for the Iida and Hiroshima test areas. (A) Large range (r = 35 to r = 0.1 km) view of box-counting behavior for the active faults of the Iida area. Vertical lines mark the 18.4 to 2.84 km range analyzed by Hirata (1989). (B) Data from the 17.5 to 2 km ranges are shown in detail. Scaling parameters computed over the 17.5-7.5 km and 7.5-2 km range are noted. (C) and (D) illustrate features of the log$N$/log$r$ plot from the Hiroshima area. Modified from Wilson and Nishizawa (1998).

Figure 6: Variations in D_L and D_S are shown along Lines 1 through 3. ATL = Akaishi Tectonic Line. ISTL = Itoigawa Shizuoka Tectonic Line. (A) Line 1 ends in central Japan. (B) Line extends along the entire length of Honshu. (C) Line 3 extends along the entire length of Honshu.

Figure 7: Plots of the relation between the capacity dimension and seismic b-value. (A) Line 1. (B) Line 2. (C) Line 3.

Figure 8: The correlation coefficients between b and D_S computed along Lines 1 through 3 are contoured to illustrate the spatial distribution of positive correlation regions (Areas I through III) throughout Japan.

Figure 9. Areas of positive correlation between b and D (Areas I through III) are located on this seismicity map.

Figure 10. Spatial map showing the distribution of maximum observed earthquake magnitude throughout Japan.

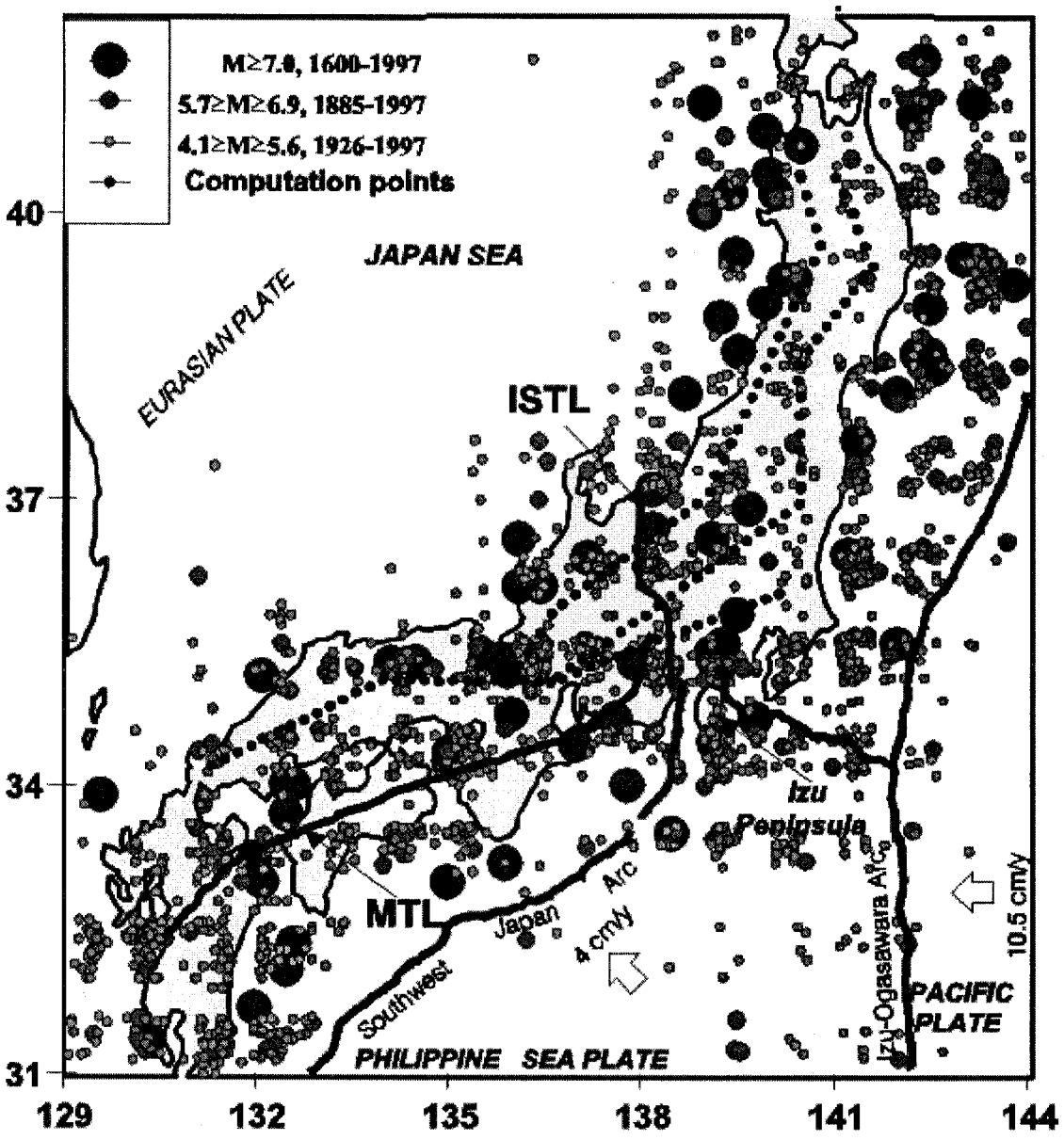

Figure 1. **Shallow seismicity data (h < 20 km) on land covering the period of time from 1600 to 1997.**

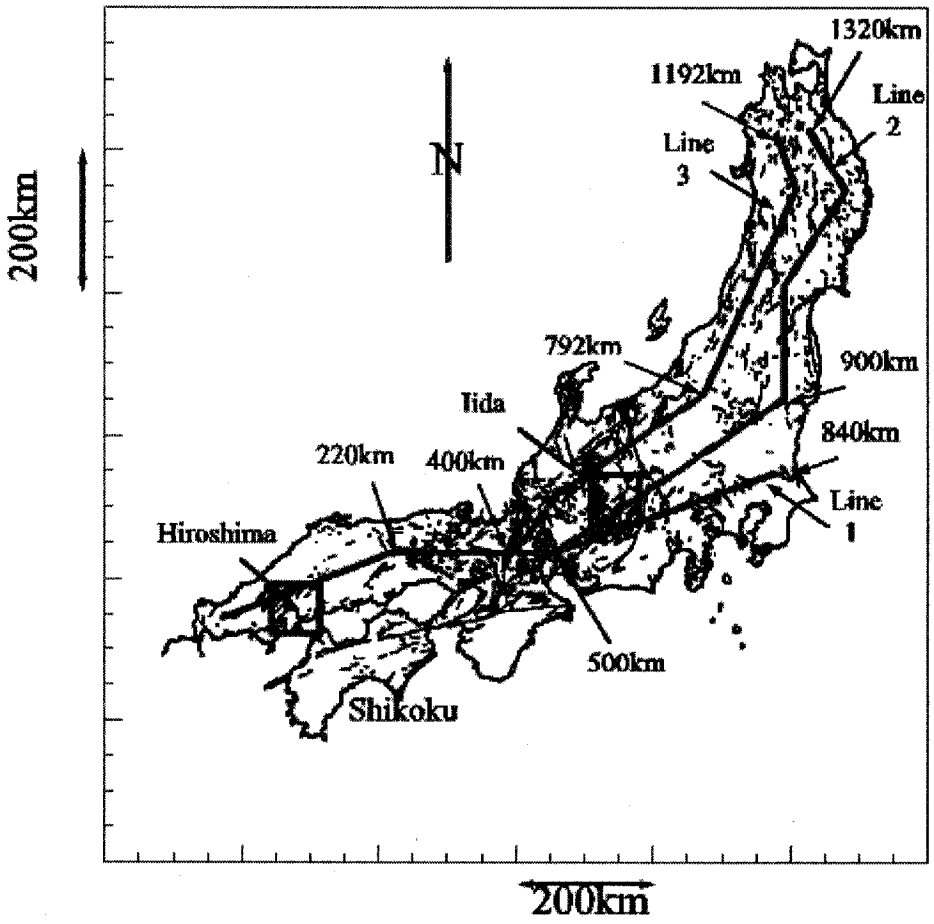

Figure 2. **Active fault map of Honshu and Shikoku. Locations of analysis Lines 1 through 3 are shown.**

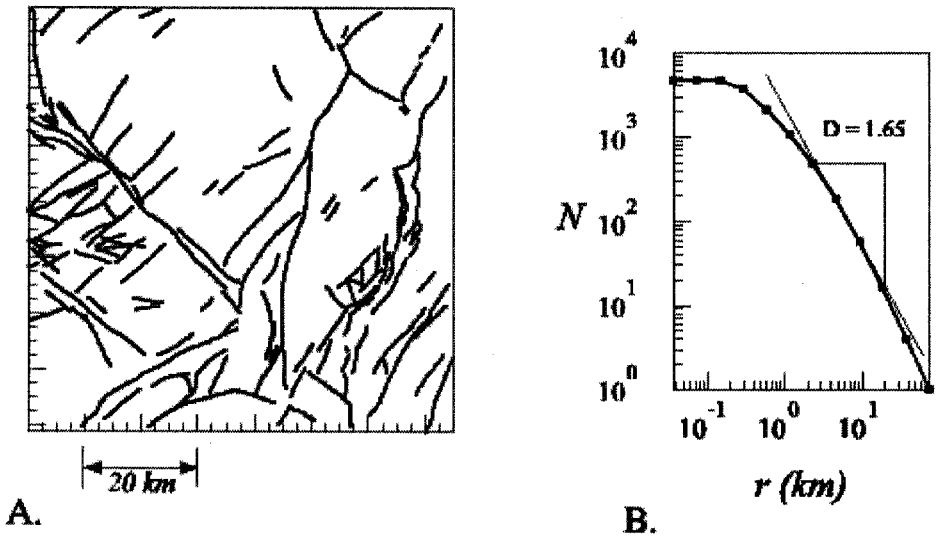

Figure 3. **(A) Active faults of the Iida area located in centra Japan (Figure 1). (B) log*N*/log*r* plot of the active fault network in Iida.**

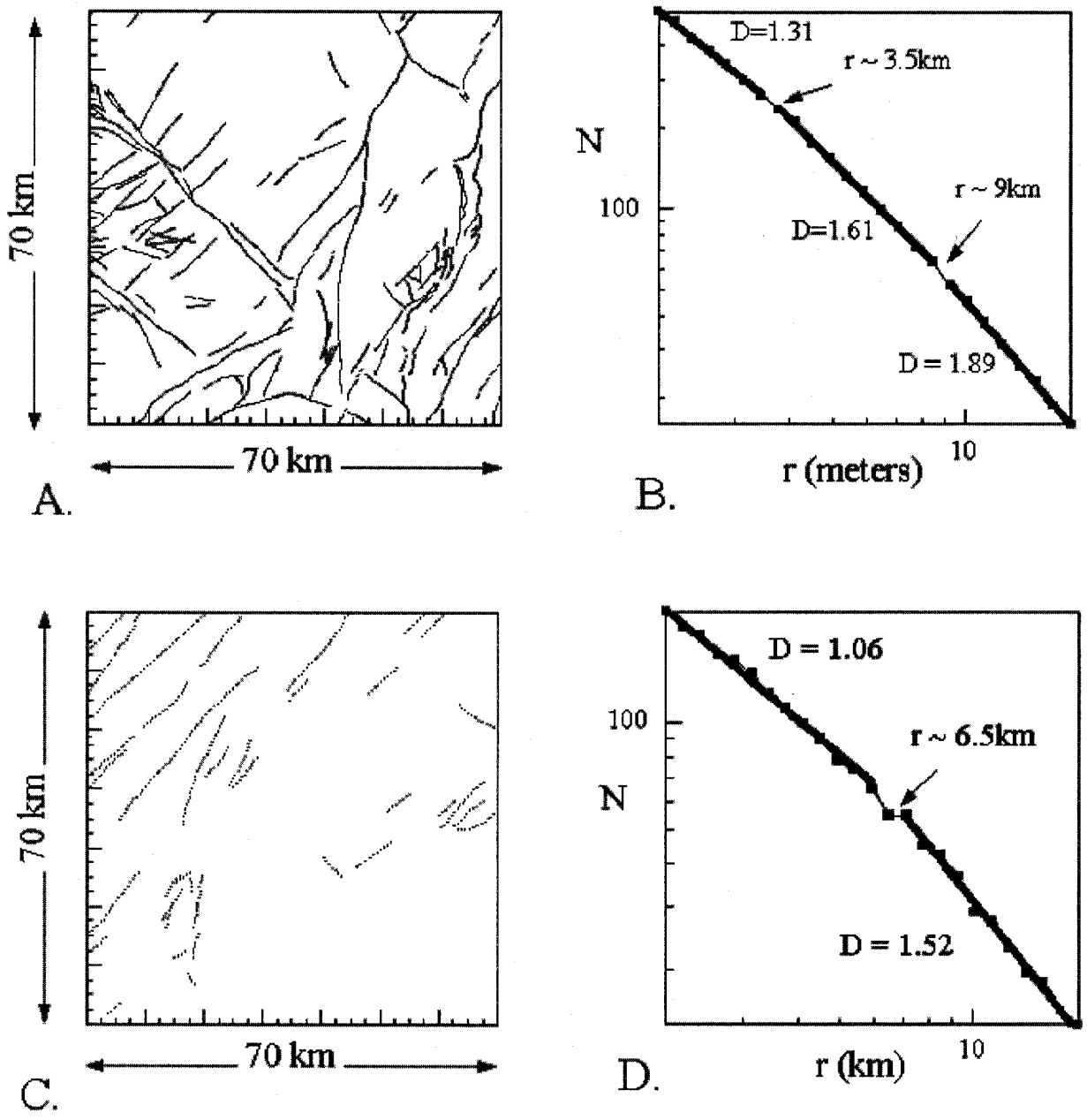

Figure 4. **(A)Active faults of the Iida area in central Japan (see Figure 2). (B) Box curve of the active fault network in Iida. (C) Active fault pattern in the Hiroshima area. (D) Box curve for the active faults mapped in Hiroshima area. (After Wilson (in review)).**

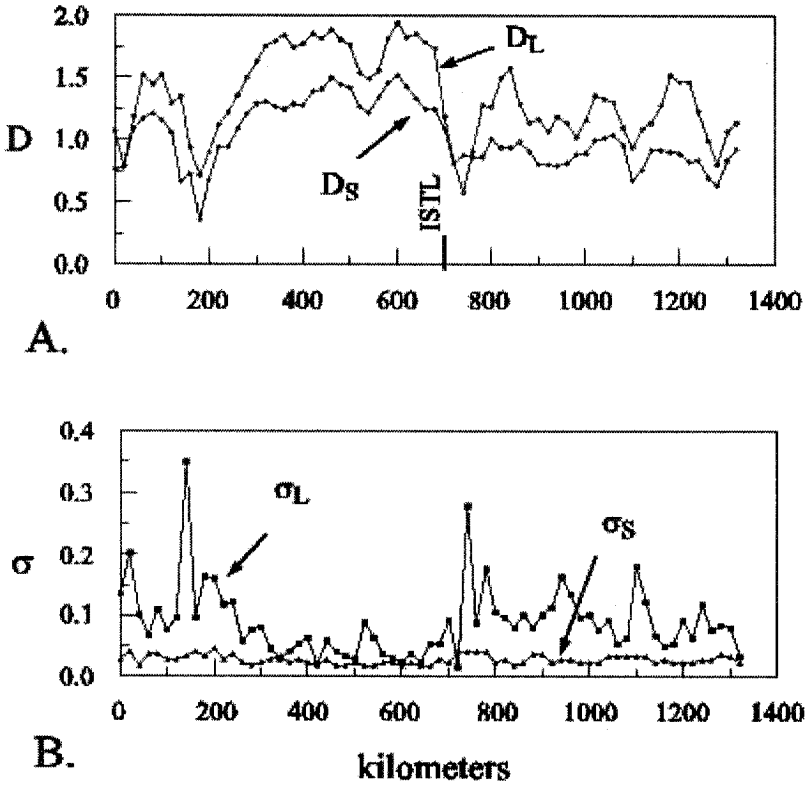

Figure 5. **(A) Range-limited fractal dimensions D_s and D_L are compared. (B) Standard deviations s_s and s_r in the estimates of D_s and D_L respectively, are compared.**

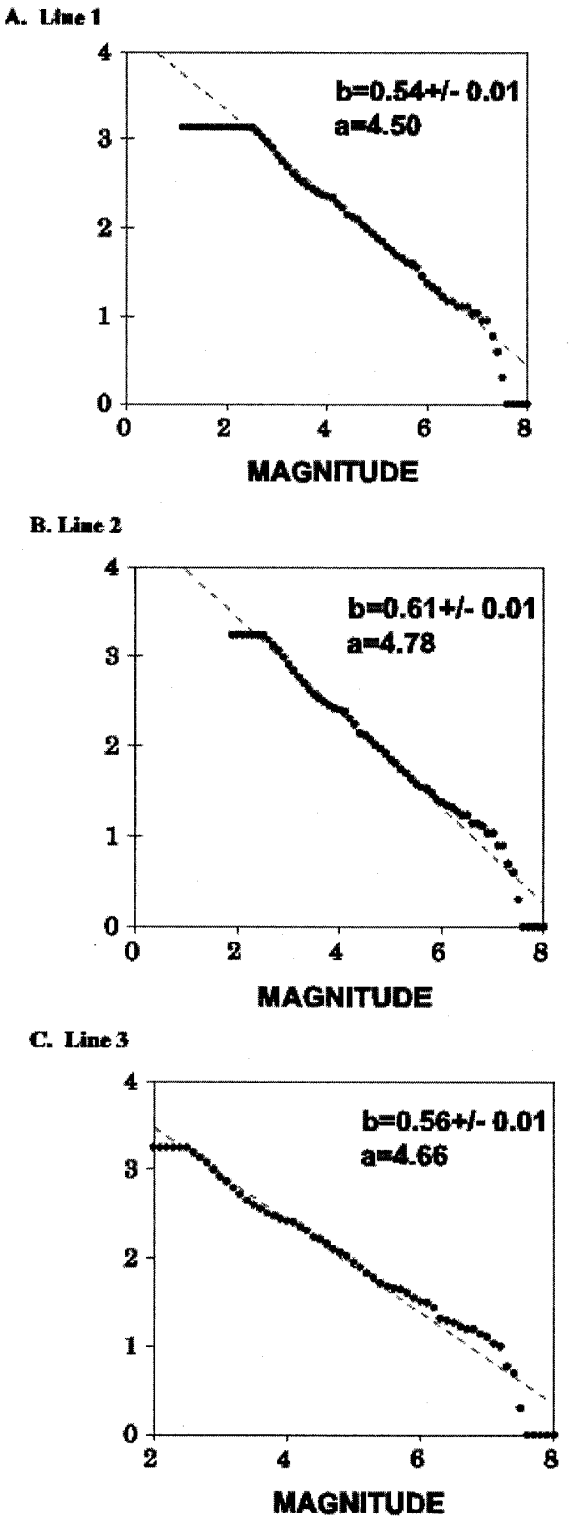

Figure 6. **Frequency-magnitude distributions for 100 km wide bands of seismicity centered on each of lines through 1 to 3..**

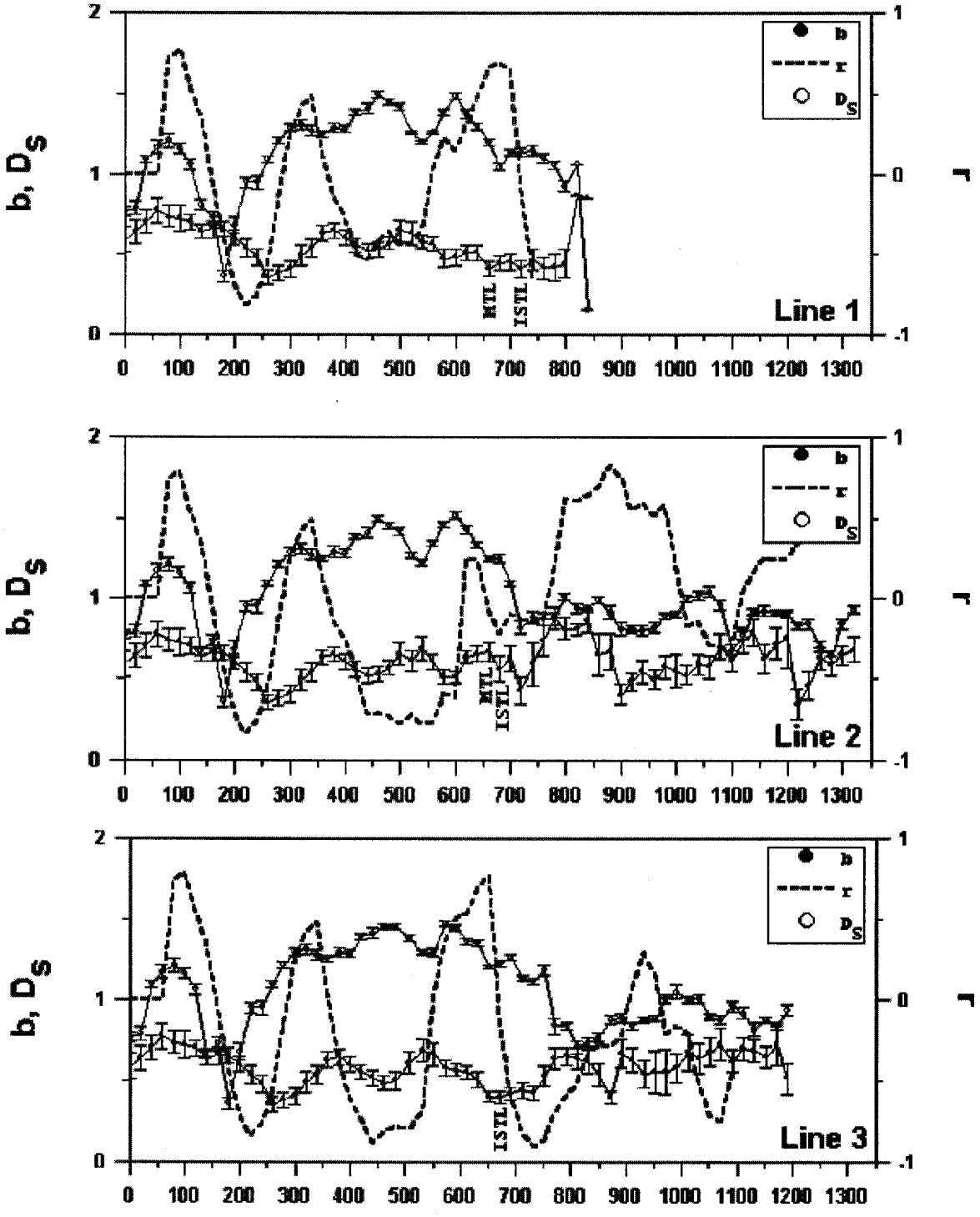

Figure 7. **Variations in D_L and D_S are shown along Lines 1 through 3. MTL = Median Tectonic Line. ISTL = Itoigawa Shizuoka Tectonic Line. (A) Line 1 ends in central Japan. (B) Line 2 extends along the entire length of Honshu and is located to the east in northern Honshu. (C) Line 3 also extends along the entire length of Honshu, but is located to the west in northern Honshu.**

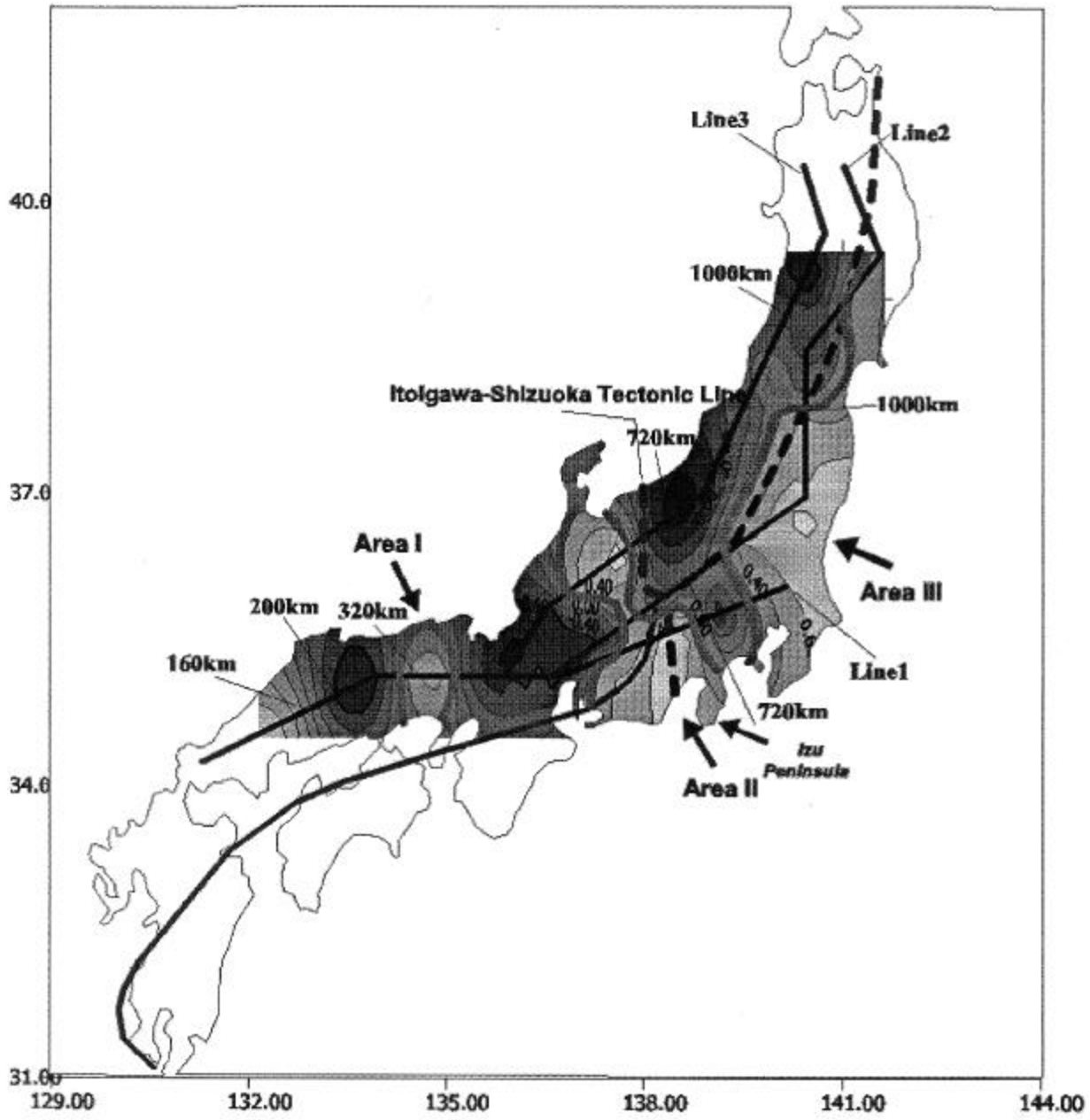

Figure 8 **The correlation coefficients between *b* and *Ds* computed along Lines 1 through 3 are contoured to illustrate the spatial distribution of positive and negative correlation regions throughout Japan.**

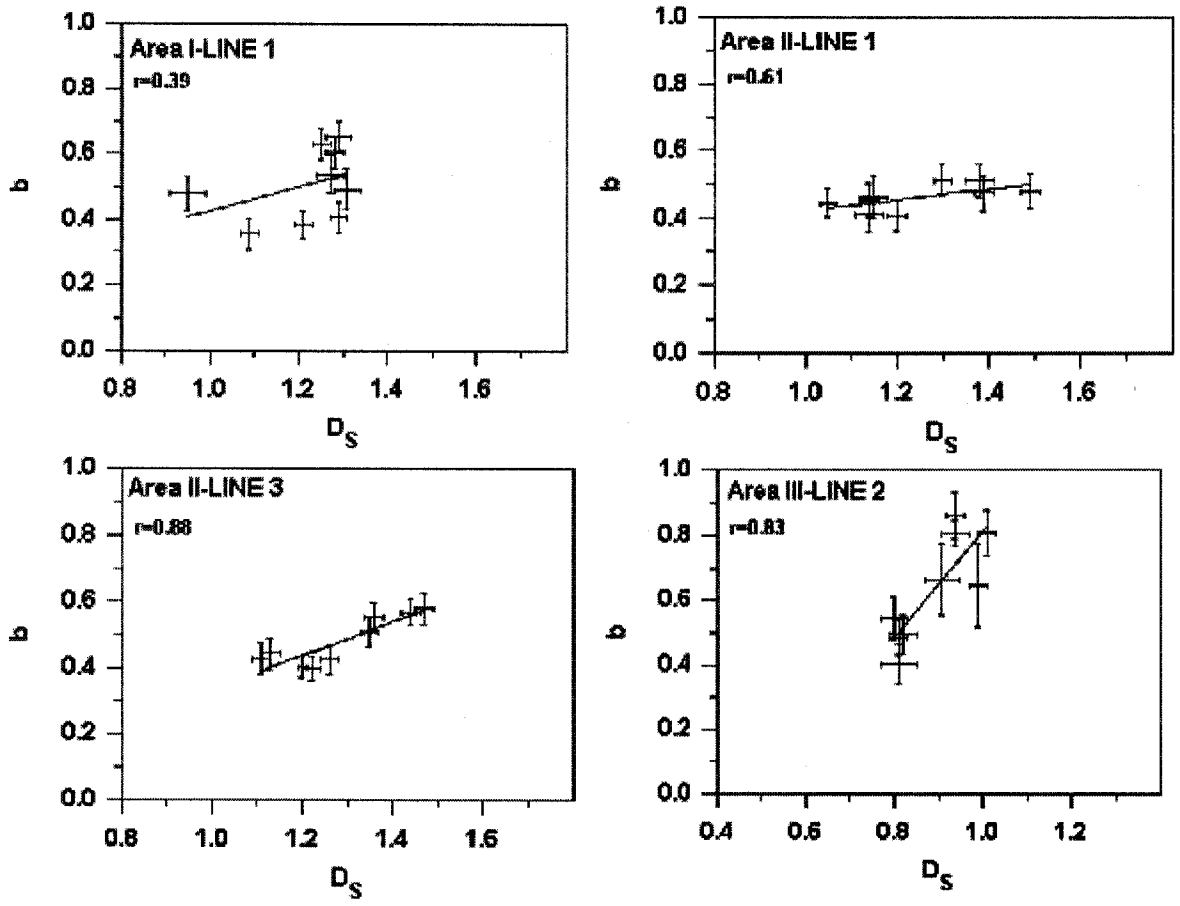

Figure 9. Plots of the relation between D_s and seismic b for the Areas of I, II, and III.

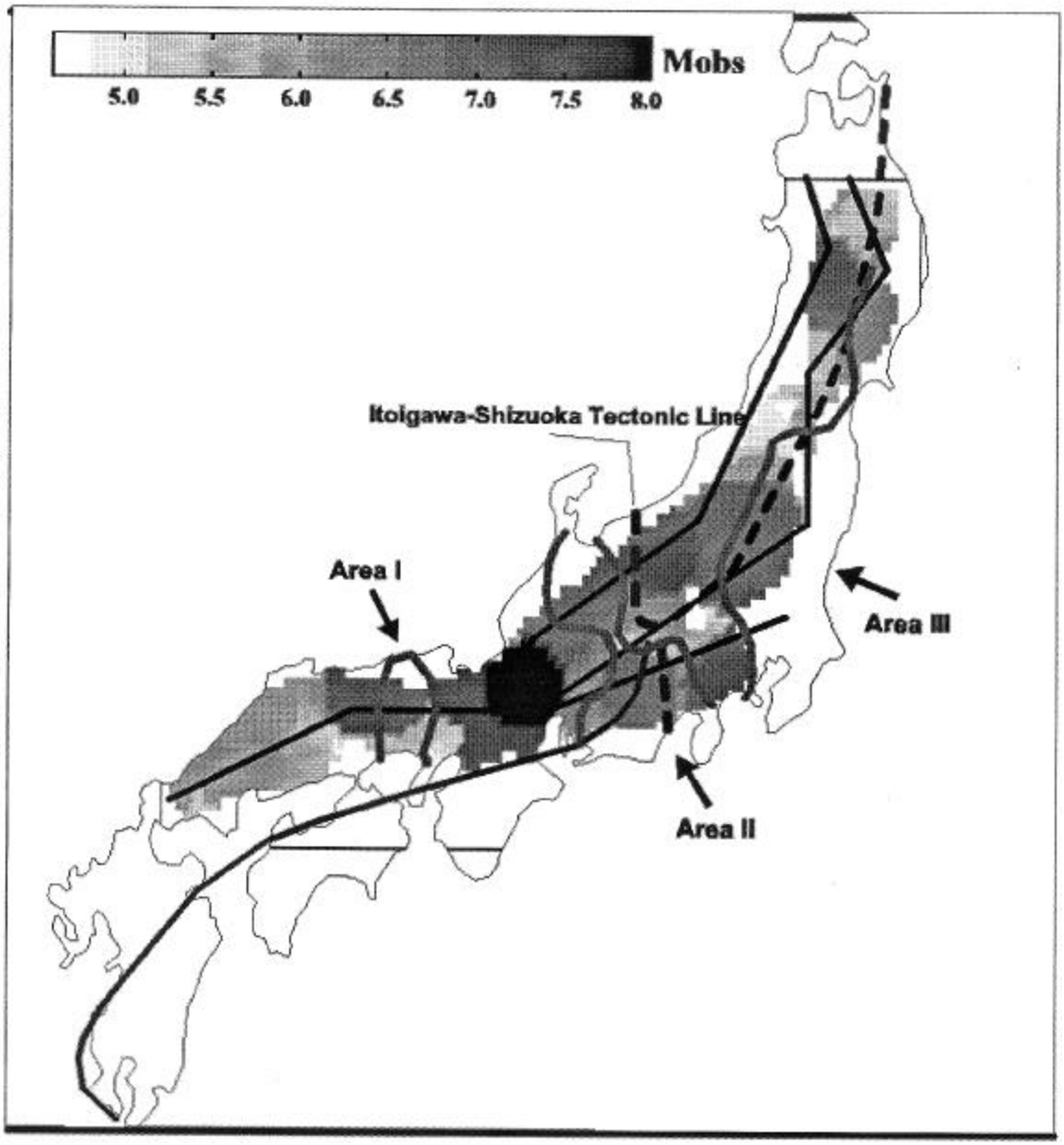

Figure 10. Spatial map showing the distribution of maximum observed earthquake magnitude throughout Japan.